remote sensing

MDPI

Article

Research and Design of BPM Shortwave Time Signal Modulation Technology Based on Chirp

Jiangbin Yuan [1,2,3], Shifeng Li [1,3,4,*], Wenhe Yan [1,3], Yuhang Song [5], Chaozhong Yang [1,3,4], Zhaopeng Hu [1,3,4], Dafeng Yang [6] and Yu Hua [1,3,4]

1 National Time Service Center, Chinese Academy of Sciences, Xi'an 710600, China; yuanjiangbin@ntsc.ac.cn (J.Y.); ywh@ntsc.ac.cn (W.Y.); ycz@ntsc.ac.cn (C.Y.); huzhaopeng@ntsc.ac.cn (Z.H.); hy@ntsc.ac.cn (Y.H.)
2 Laboratory of Science and Technology on Marine Navigation and Control, China State Shipbuilding Corporation, Tianjin 300131, China
3 Key Laboratory of Time Reference and Applications Chinese Academy of Sciences, Xi'an 710600, China
4 University of Chinese Academy of Sciences, Beijing 100049, China
5 Tianjin Navigation Instrument Research Institute, Tianjin 300131, China; songyuhang@tju.edu.cn
6 Xi'an Air-Space Electronic Technology Co., Ltd., Xi'an 710061, China; ydf_dafeng@163.com
* Correspondence: lishifeng@ntsc.ac.cn

Abstract: The shortwave time service system is a vital land-based wireless time service solution, serving as a supplement and backup to the global navigation satellite system. It ensures that time users can access reliable timings, especially in extreme situations. However, the current BPM shortwave time service signal in China faces issues such as insufficient anti-interference reception capabilities and poor timing accuracy. This paper capitalizes on the advantages of Chirp signals and explores a new modulation technology for BPM shortwave time signals that is compatible with the existing modulation system. A Dual Chirp Time-Division Combined Modulation (DCTDCM) scheme is proposed for broadcasting two time signals: Coordinated Universal Time (UTC) and Universal Time 1 (UT1). Furthermore, an in-depth study of the receiving method for this scheme is conducted, with detailed design of its parameters. The designed DCTDCM signals offer a spread spectrum gain of 24 dB and a multipath resolution capability of at least 125 µs, significantly enhancing the anti-interference reception and anti-multipath attenuation capabilities of shortwave time signals. As a result, the availability and timing accuracy of shortwave time signals are substantially improved. Finally, extensive comparative experiments on reception performance validate the effectiveness of this approach.

Keywords: shortwave time service; BPM; time signals; modulation; chirp signal

Citation: Yuan, J.; Li, S.; Yan, W.; Song, Y.; Yang, C.; Hu, Z.; Yang, D.; Hua, Y. Research and Design of BPM Shortwave Time Signal Modulation Technology Based on Chirp. *Remote Sens.* **2024**, *16*, 4035. https://doi.org/10.3390/rs16214035

Academic Editor: Giuseppe Casula

Received: 5 September 2024
Revised: 18 October 2024
Accepted: 23 October 2024
Published: 30 October 2024

1. Introduction

The time service system, as a critical component of the time–frequency infrastructure, plays a key role in supporting societal development and ensuring national security [1–4]. It is one of the most vital infrastructures for any country. With the advancement of Global Navigation Satellite Systems (GNSSs), satellite-based time services have become the primary method of modern time synchronization. However, GNSS signals are susceptible to interference, obstructions, and deception, highlighting an inherent vulnerability in relying solely on this system [5–7]. A single GNSS time service system may not be sufficient to ensure the security, reliability, and robustness required for the national time service infrastructure [8].

On 10 May 2017, the U.S. website *Defense One* published an article titled "*Time War: The Threat to GPS Is More Than Navigation and Positioning*", emphasizing the critical importance of timing information in Positioning, Navigation, and Timing (PNT) systems. Furthermore, on 4 December 2018, U.S. President Donald Trump signed the "*National Security and Resilient*

Time Act", underscoring the necessity of establishing a reliable alternative time service system to supplement Global Positioning Satellite System (GPS) satellites for national and economic security. Unlike GNSS, shortwave time service offers irreplaceable advantages, such as long-range operability and robustness during wartime [9,10], making it a reliable backup and supplementary solution for GNSS-based time services.

At present, there are a total of nine shortwave time service broadcasting stations worldwide, identified by their call letters and countries: BPM/China, WWV/United States, WWVH/United States, RWM/Russia, CHU/Canada, EBC/Spain, HLA/South Korea, LOL/Argentina, and MIKES/Finland. However, since the introduction of shortwave time services in the early 20th century, the research on and development of shortwave time signal modulation methods have remained largely stagnant. In recent years, only one study has explored the feasibility of a spread spectrum system for shortwave time signal broadcasting, but it neither specified which spread spectrum technology was used nor provided a parameter design method for the new time signal scheme [10]. Despite technological advances, BPM shortwave time service still employs the relatively outdated amplitude modulation (AM) method to broadcast time signals, lacking significant innovation and breakthroughs.

With the continuous development of the information age, the electromagnetic environment of the shortwave channel has become increasingly complex [11]. This includes challenges such as multipath interference, fading, and Doppler frequency shifts [12–14], as well as a growing amount of interference from radio stations and industrial sources. Existing shortwave time signal modulation methods have struggled to maintain the performance required for reliable time service.

The most effective way to enhance the performance of shortwave time service is through the research and design of a new modulation method with strong anti-interference reception capabilities and high signal detection accuracy. In view of the advantages of linear frequency modulation signals (Chirp signals), such as their low power consumption, strong anti-interference ability, and strong resistance to Doppler frequency shift and multipath fading, Chirp signals have been studied and applied in many fields [15–22]. Ref. [15] reports the use of broadband Chirp signals for spread-spectrum communication in indoor and industrial environments. Ref. [16] studies the accurate synchronization method using Chirp signals in the fractional Fourier domain. Ref. [17] proposes a new communication system based on Chirp signals to try to solve the problem of common synchronization methods being affected by channels in broadband and ultra-wideband situations. Ref. [18] studies an orthogonal multi-carrier underwater acoustic communication system based on fractional Fourier transform for complex underwater acoustic channels. Ref. [19] proposes and implements a subspace-based two-way ranging system for high-resolution indoor ranging based on Chirp spread spectrum signals. This system is robust to frequency offset. Ref. [20] proposes a novel method for detecting and estimating the distance, velocity, and direction of arrival of multiple far-field targets using broadband Chirp signals. Ref. [21] proposes a Dual-Mode Chirp Spread Spectrum (DM-CSS) modulation for low-power wide-area networks for data modulation. DM-CSS modulation has high spectral efficiency and has good bit error rate performance in additive white Gaussian noise channels, fading channels, and in the presence of phase and frequency offsets. Ref. [22] points out that CSS modulation is the most important technology in long-distance radio communication. These studies fully demonstrate that introducing linear frequency modulation signals into shortwave time signal modulation is expected to significantly improve the anti-interference reception ability and signal detection accuracy of shortwave time service terminals, thus addressing the increasing demand for higher service quality.

This paper fully leverages the advantages of Chirp signals and, while maintaining compatibility with the existing BPM shortwave time signal modulation, conducts research on a new BPM shortwave time signal modulation technology. It introduces a Dual Chirp Time-Division Combined Modulation (DCTDCM) scheme for broadcasting two shortwave time signals, Coordinated Universal Time (UTC) and Universal Time 1 (UT1). Additionally, an in-depth study on the reception method of this scheme is conducted, taking into

account the frequency difference time shift characteristics of Chirp signals and the specific characteristics of the shortwave channel. The parameters of this new scheme are meticulously designed.

This paper is organized as follows. In Section 2, we briefly introduce the existing BPM shortwave time service technology. In Section 3, we conduct a detailed study of DCTDCM, mainly including modulating baseband signals, modulation schemes, receiving methods, and parameter design. In Section 4, comprehensive comparative measurement experiments related to reception performance were conducted across several locations in China, including Pucheng County, Luonan County, Xi'an City, Xuyi County, Changchun City, Sanya City, and Kashgar City, verifying the effectiveness of our proposed method. Finally, brief discussions and conclusions are presented in Sections 5 and 6.

2. Existing BPM Shortwave Time Service Technology

The shortwave time service system transmits time information through time signals. The specific implementation involves establishing a correlation between the start of the broadcast time signals and the standard time, allowing users to determine timing by detecting the arrival of these signals. China's BPM shortwave time service system utilizes four carrier frequencies: 2.5, 5, 10, and 15 MHz. The available total bandwidths are 10, 10, 10, and 20 KHz, respectively.

Following a specific broadcasting procedure, current technology transmits BPM shortwave time signals, standard frequency signals (empty carriers), and BPM call letters at designated intervals. The system provides time service coverage extending over 3000 km, with time service accuracy to the order of milliseconds.

The BPM shortwave time service system is the only time service system in China that broadcasts both UTC and UT1 time signals. The AM used by the system is described by the following equation:

$$S_{AM}(t) = \begin{cases} A[1 + m \cdot \sin(2\pi f_b t)] \sin(2\pi f_0 t) & 0 \le t < T_{AM} \\ A \sin(2\pi f_0 t) & T_{AM} \le t < 1 \text{ s}, \end{cases} \quad (1)$$

where A is the carrier amplitude, m is the modulation index, $f_b = 1$ kHz, f_0 is the carrier frequency, and T_{AM} controls the duration of the baseband signal. T_{AM} characterizes different types of time signals and is defined as follows:

(1) When $T_{AM} = 10$ ms, it represents the second signal in the UTC signals.
(2) When $T_{AM} = 100$ ms, it represents the second signal in the UT1 signals.
(3) When $T_{AM} = 300$ ms, it represents the whole minute signal.

UTC signals were emitted in advance on UTC by 20 ms and emitted from minutes 0 to 10, 15 to 25, 30 to 40, and 45 to 55. UT1 signals are emitted from minute 25 to 29, and 55 to 59.

3. Materials and Methods

3.1. Research and Design of New BPM Shortwave Time Signal Modulation Scheme

3.1.1. Overall Design Scheme

In this study, the DCTDCM scheme is applied to the BPM time service system. See Section 3.1.4 for details. During the research and development process of the DCTDCM scheme, the following basic principles were adhered to:

- Principle 1: The new time signal modulation must not interfere with the normal broadcasting of the time signals in the existing system or the regular operation of users within the current system.
- Principle 2: The new time signal modulation must meet system bandwidth requirements and should not increase the system's transmission power.
- Principle 3: The new time signal modulation must effectively enhance the anti-interference reception capability and improve the timing accuracy of the receiving terminal.

- Principle 4: The new time signal modulation must facilitate the basic timing function of modulating two shortwave time signals: UTC and UT1.
- Principle 5: The extended application potential of the system must also be considered.

Based on these principles, this paper proposes an overall design scheme that incorporates the DCTDCM signals into the empty carrier section of the existing time signal modulation, as illustrated in Figure 1.

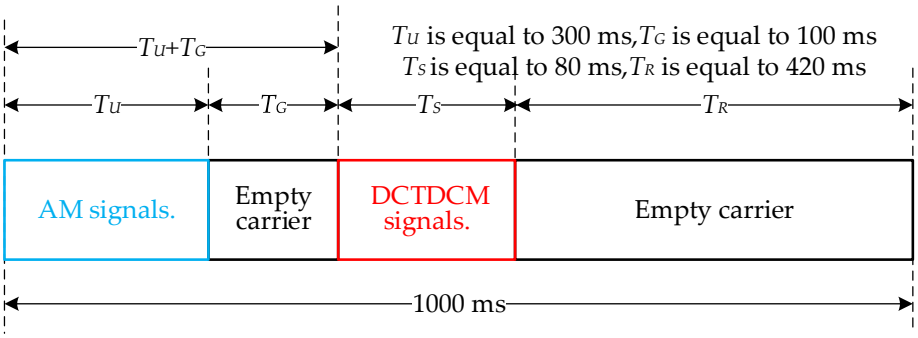

Figure 1. Schematic of the overall design scheme.

For principle 1, the duration T_U occupied by the AM signals is designed to be a maximum of 300 ms to ensure the uninterrupted broadcasting of the AM signals. Additionally, to eliminate any potential interference from the DCTDCM signals on existing users, an isolation interval T_G of 100 ms is incorporated.

For principle 2, the bandwidth of the DCTDCM signals is designed as 8 kHz (with 1 kHz reserved on each side of the spectrum, so that most of the signal energy is concentrated within the band. See Section 3.1.2 for details) to meet the system bandwidth requirements and serves as a constant envelope without increasing the transmission power.

For principle 3, using Chirp signals as the baseband signal in the DCTDCM can effectively enhance the anti-interference reception capability and timing accuracy of the receiving terminal. See Section 3.1.3 for details.

For principle 4, DCTDCM uses two Chirp signals to realize the modulation of UTC and UT1 time signals. See Section 3.1.4 for details.

For principle 5, the total time length T_S of the DCTCDM is designed to reserve an empty carrier with a time length of 420 ms to support the subsequent research on shortwave data modulation technology and expand the system application.

Furthermore, the broadcasting times of the four carrier frequencies, as well as the broadcasting procedures of the various signals in the existing BPM shortwave timing system, remain unchanged.

3.1.2. Baseband Signal

The performance quality of time signal modulation is closely related to the baseband signal used. Spread spectrum signals are widely applied in both military and civil communication systems owing to their strong anti-interference capabilities, resistance to multipath fading, and high measurement accuracy [23–29]. These signals have also demonstrated remarkable success in applications such as GPS and the BeiDou Navigation Satellite System (BDS). As a result, using spread spectrum signals as the baseband signal for shortwave time signal modulation can significantly improve the anti-interference reception capabilities and timing accuracy of receiving terminals.

Chirp signal and Direct Sequence Spread Spectrum (DSSS) signals are two of the most commonly used spread spectrum signals. DSSS signals, commonly used in GPS and BDS, are favored for their ease of implementation in code division multiple-access systems. However, under identical conditions of duration and bandwidth, Chirp signals outperform DSSS signals in terms of spectral characteristics, autocorrelation, and resistance to carrier frequency offset, making them more suitable for shortwave timing systems.

For further explanation, consider a signal with a duration of 31.75 ms and a bandwidth of 8 kHz.

In terms of spectral characteristics, the spectrum of the Chirp signal is flatter, with more concentrated energy, as shown in Figure 2. Through numerical calculations, the in-band energy proportions of DSSS and Chirp signals are 90.76% and 99.82%, respectively. For shortwave timing systems, which have limited bandwidth resources, the in-band energy proportion is a crucial metric. The higher the energy proportion, the greater the allowable signal design bandwidth, and the more efficiently the bandwidth resources are utilized.

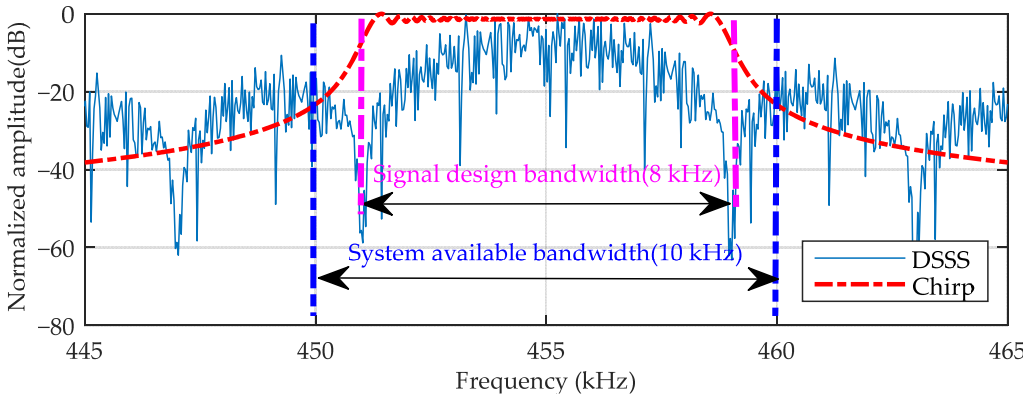

Figure 2. Spectrum diagrams of the DSSS and Chirp signals.

In terms of autocorrelation, the main lobe of the autocorrelation peak for Chirp signals is sharper, with a main lobe width that is only half that of the autocorrelation peak for DSSS signals, as illustrated in Figure 3. This indicates that, under the same duration and bandwidth, the multipath resolution capability and spread spectrum gain of Chirp signals are superior to those of DSSS signals.

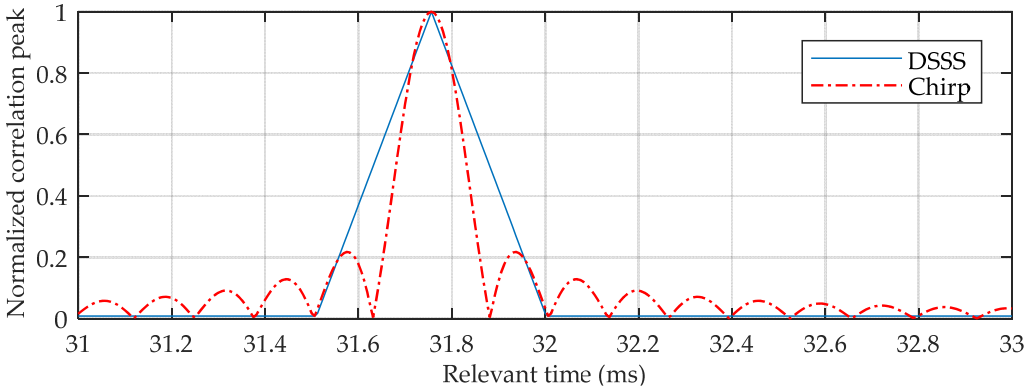

Figure 3. Autocorrelation functions of DSSS and Chirp signals.

In terms of resistance to carrier frequency offset, the relationship between the attenuation of the autocorrelation peak for DSSS signals and the carrier frequency offset can be expressed as $\alpha = -20\log 10(|\sin c(Tf_d)|)$, where T is the signal duration. From this, it can be seen that when f_d is large, the autocorrelation peak of DSSS signal will experience severe attenuation. In contrast, the carrier frequency offset has very little effect on the autocorrelation peak of the Chirp signal, as shown in Figure 4.

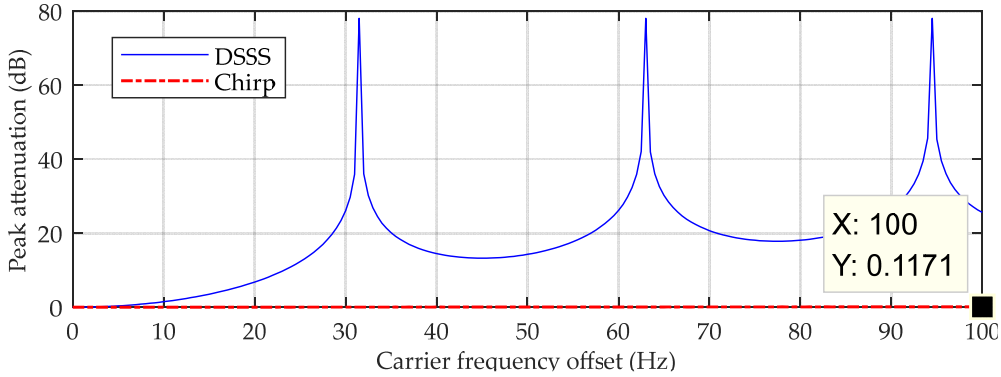

Figure 4. Influence of carrier frequency offset on autocorrelation function.

3.1.3. Time Shift Characteristic of Frequency Difference in Chirp Signal

In this section, we examine the frequency difference–time shift (FD-TS) characteristic of Chirp signals. This characteristic explains the internal mechanism behind the Chirp signal's resistance to carrier frequency offset. By designing two Chirp signals with opposite Chirp rates using this characteristic, joint measurement of signal arrival time and carrier frequency offset can be achieved, laying the groundwork for further research on the DCTDCM scheme.

The Chirp signal (baseband signal) without carrier frequency offset is defined as follows:

$$C_i(t) = A\exp\left[\mathrm{j}(-1)^i\left(K\pi t^2 - \pi Bt\right)\right] \tag{2}$$

where A is the signal amplitude and its value is equal to the carrier amplitude of the AM signal, j is the imaginary unit, $i \in [1,2]$ characterizes the polarity of the Chirp rate, $K = B/T$ represents the numerical value of the Chirp rate, and B and T respectively represent the duration and bandwidth of the Chirp signal. Then, the Chirp signal after introducing the carrier frequency offset is denoted as $C'_i(t) = \exp(-j2\pi f_d t)C_i(t)$, where f_d is the carrier frequency offset. The conjugate signal $\overline{C}_i(t)$ of $C_i(t)$ is used to perform matched autocorrelation reception on $C_i(t)$. $S(\tau)$ is used to represent the autocorrelation peak output by the matched filter at time τ. Thus, we can obtain

$$\begin{aligned} S(\tau) &= A\left\|\int_0^T \exp(-\mathrm{j}2\pi f_d t)\cdot C_i(t)\cdot\overline{C}_i(t+\tau)\mathrm{d}t\right\| \\ &= A\left\|\int_0^T \exp\left[-\mathrm{j}2\pi f_d t + \mathrm{j}(-1)^i\left(K\pi t^2 - \pi Bt\right) - (-1)^i\left(K\pi(t+\tau)^2 - \pi B(t+\tau)\right)\right]\mathrm{d}t\right\| \\ &= A\left\|\int_0^T \exp\left[\mathrm{j}2\pi\left(-f_d t + (-1)^{i-1}K\tau t\right)\right]\mathrm{d}t\right\| \end{aligned} \tag{3}$$

Equation (3) shows that when $-f_d t + (-1)^{i-1}K\tau t = 0$, i.e., when $\tau = (-1)^{i-1}f_d/K$, $S(\tau)$ obtains the maximum autocorrelation peak (MAP). This indicates that the MAP of the Chirp signal is independent of the carrier frequency offset, but the time at which it appears is related to the carrier frequency offset and the Chirp rate.

According to the above analysis, we design two Chirp signals with opposite Chirp rates according to Equation (2), which are $C_1(t)1$ and $C_2(t)$, respectively. When there is no carrier frequency offset, the times at which the MAP of $C_1(t)$ and $C_2(t)$ appear are assumed to be τ_1 and τ_2, respectively. When there is a carrier frequency offset, the time at which the MAP of $C_1(t)$ appears will be shifted by $-f_d/K$ relative to (τ_1 means shifting to the left, $f_d < 0$ means shifting to the right), and the time at which the MAP of $C_2(t)$ appears will be shifted by f_d/K relative to τ_2 ($f_d > 0$ means shifting to the right; $f_d < 0$ means shifting to the left). In other words, the time shifts of the AMP of $C_1(t)$ and $C_2(t)$ caused by the carrier frequency offset are always mirror-symmetrical about their central time $t_m = (\tau_1 + \tau_2)/2$, as illustrated in Figure 5. Therefore, by performing correlation reception on $C_1(t)$ and

$C_2(t)$ using matched filtering, the joint measurement of both signal arrival time and carrier frequency offset can be straightforwardly achieved. The implementation method is detailed in Section 3.2.3.

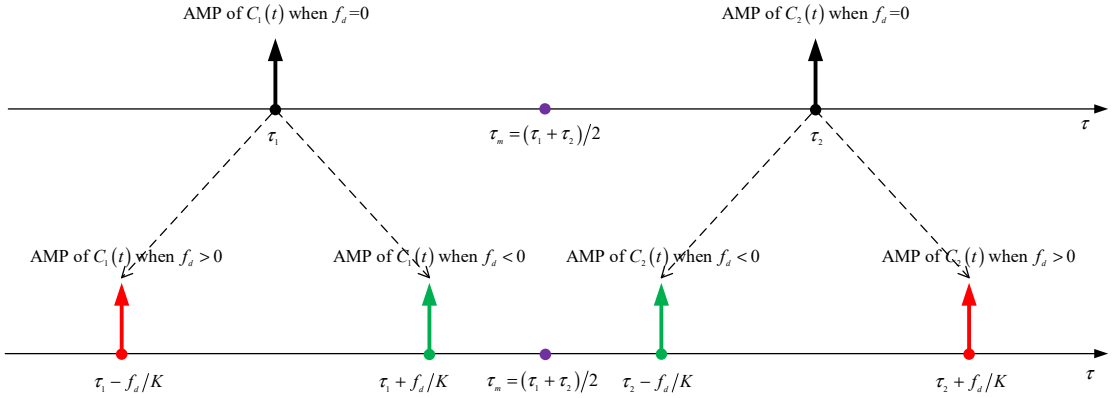

Figure 5. Schematic of the FD-TS characteristic for Chirp signal.

3.1.4. Modulation Scheme

Based on the FD-TS characteristic of Chirp signals, this paper proposes the DCTDCM scheme for transmitting two time signals: UTC and UT1. This scheme is illustrated in Figure 6, where 1PPS_BPMC and 1PPS_BPM1 represent the UTC second start time and UT1 s start time, respectively, in the BPM shortwave time service system. In the DCTDCM scheme, there are two Chirp signals with opposite Chirp rates, namely $C_1(t)$ and $C_2(t)$. Their definition formulas are as shown in Equation (2).

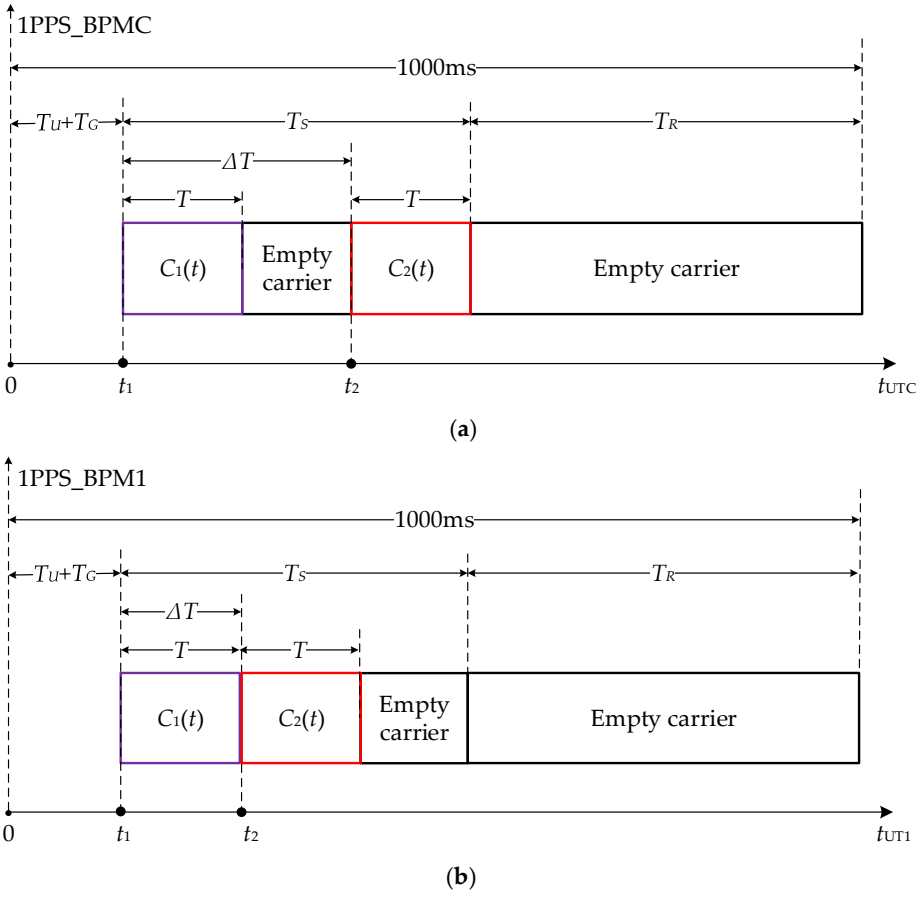

Figure 6. Basic structure of the DCTDCM scheme: (**a**) UTC signal modulation scheme; (**b**) UT1 time signal modulation scheme.

The time interval between the start of broadcasting $C_1(t)$ and the start of broadcasting the $C_2(t)$ is denoted as ΔT. For simplicity, we describe ΔT as the relative broadcasting time interval between the two Chirp signals. Different values of ΔT can be used to represent different types of time signals. In this paper, it is stipulated that during the UTC signal broadcasting period, $\Delta T = T_S - T$, and during the UT1 time signal broadcasting period, $\Delta T = T$.

3.2. Research on Receiving Method Based on Matched Filtering

3.2.1. Basic Principle

Conventional receiving methods for Chirp signals include transform domain detection techniques such as Chirp-Fourier transform [30–32] and fractional Fourier transform [16,18,33–36]. These methods collect the energy of Chirp signals in the frequency or fractional domain for peak detection. However, owing to limitations in frequency or fractional domain resolution, the peak detection accuracy of these methods is not high, making it challenging to achieve precise timing. Additionally, their implementation complexity is relatively high.

Based on the characteristics of the DCTDCM, this paper proposes two matched filters to perform correlation reception on $C_1(t)$ and $C_2(t)$. The first matched filter is designed to match $C_1(t)$, with the resulting correlation peak denoted as $S_1(\tau)$. The second matched filter is designed to match $C_2(t)$, with the resulting correlation peak denoted as $S_2(\tau)$, as shown in Figure 7.

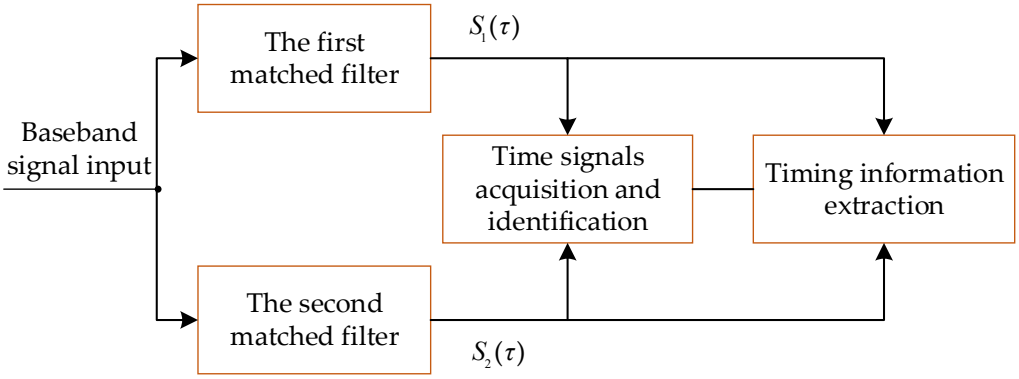

Figure 7. Basic principle based on matched filter reception.

Let $\widetilde{\tau}_i (i = 1,2)$ represent the time of the ith matched filter output (MAP), i.e., $\widetilde{\tau}_i$ is the time when $S_i(\tau)$ reaches the MAP. Let $\Delta\widetilde{\tau} = \widetilde{\tau}_2 - \widetilde{\tau}_1$ represent the relative time interval when $S_1(\tau)$ and $S_2(\tau)$ reach the MAP. According to different values of $\Delta\widetilde{\tau}$, time signal acquisition and identification can be achieved, and their implementation method is described in Section 3.2.2. According to $\Delta\widetilde{\tau}$, timing information extraction can also be achieved, and its implementation method is described in Section 3.2.3.

3.2.2. Time Signal Acquisition and Identification Method

Based on the basic principle of matched filter reception, this section proposes a method called Maximum Peak Relative Time Interval Decision (MPRTID) to achieve time signal acquisition and type identification.

According to the FD-TS characteristic of Chirp signals, when the carrier frequency offset is unknown, the value of the maximum peak relative time interval $\Delta\widetilde{\tau}$ is uncertain. Therefore, in the MPRTID method, we define two value sets of $\Delta\widetilde{\tau}$. One is the judgment domain of UTC signals, denoted as $\mathbf{R}_{\mathrm{UTC}}$, and the other is the judgment domain of UT1 time signals, denoted as $\mathbf{R}_{\mathrm{UT1}}$. In the process of time signal acquisition and identification, the first step is to find the time at which $S_1(\tau)$ obtains the MAP and the time at which $S_2(\tau)$ obtains the MAP within each second, respectively. This allows us to calculate $\Delta\widetilde{\tau} = \widetilde{\tau}_2 - \widetilde{\tau}_1$ for each second. Finally, time signal acquisition and identification within the current second are determined according to the following three scenarios:

Case 1: If $\Delta\widetilde{\tau} \in \mathbf{R}_{\mathrm{UTC}}$, it indicates that the signal capture is successful, and the time signal type is identified as a UTC signal.

Case 2: If $\Delta\widetilde{\tau} \in \mathbf{R}_{\mathrm{UT1}}$, it indicates that the signal capture is successful, and the time signal type is identified as a UT1 time signal.

Case 3: If neither Case 1 nor Case 2 applies, no identification is made.

Currently, the most common method for signal acquisition is the threshold decision method [37]. This method compares a set detection threshold value V_t with the correlation peak V to determine whether the target signal has been captured. In the process of selecting V_t, first, an acceptable false alarm probability P_{fa} needs to be set, and the noise signal power σ_n^2 needs to be provided at the same time. Then, V_t is calculated according to P_{fa} and σ_n^2. To maintain a very small P_{fa}, the value of V_t should not be too small. However, due to the complexity of shortwave channels, selecting V_t presents two major challenges. First, shortwave channels are characterized by multipath fading, causing the correlation peak value v to fluctuate unpredictably and dynamically. When V is relatively small, if a small P_{fa} must be maintained, then V_t is very likely to be greater than the correlation V, which in turn increases the probability that weak signals cannot be detected and makes it impossible to detect an existing signal for a long time.

Second, the interference affecting the signal is not limited to receiver noise but also includes various unpredictable interferences in the shortwave channel, such as shortwave radio interference. These interferences compound the difference between the given noise signal power σ_n^2 and the actual interference power, further degrading signal detection performance.

In conclusion, when using the threshold decision method for time signal acquisition in complex shortwave channels, performance is difficult to guarantee, leading to reduced availability of shortwave time signals. In contrast, by adopting the MPRTID method proposed in this paper, a correlation peak threshold does not have to be set. As long as the autocorrelation peak value of the target signal exceeds the cross-correlation peak with the interference signal, the target signal can be captured. This resolves the challenge of effectively setting the correlation peak threshold in complex shortwave channels.

3.2.3. Timing Method

Based on the basic principle of matched filter reception and the FD-TS characteristic of Chirp signals, this section proposes a timing method using matched filtering, with the UTC signal as an example, as illustrated in Figure 8.

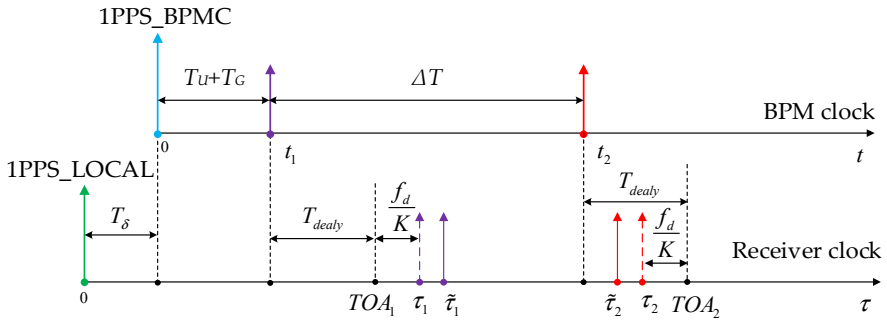

Figure 8. Timing method based on matched filtering.

At the transmitting end, the start times of the $C_1(t)$ and $C_2(t)$ transmissions are t_1 and t_2, respectively. The time difference between t_1 and 1PPS_BPMC is $T_U + T_G$, and $t_2 - t_1 = \Delta T$. At the receiving end, the times when $C_1(t)$ and $C_2(t)$ reach the receiving end after the propagation delay of T_{delay} are recorded as TOA_1 and TOA_2, respectively. Before timing is achieved, the clock difference between the local one-second signal 1PPS_LOCAL of the receiver and 1PPS_BPMC is denoted as t_1 and can be expressed as follows:

$$T_\delta = TOA_1 - (T_U + T_G) - T_{delay}. \tag{4}$$

Assuming T_{delay} has been determined, Equation (4) shows that in order to obtain the clock difference T_δ and thereby achieve timing, it is necessary to measure the arrival time TOA_1 of the $C_1(t)$ signal. Let $\tau_i (i = 1, 2)$ represent the theoretical time when the output of the ith matched filter reaches the MAP. According to the frequency difference time shift characteristic of the Chirp signal, we have

$$\begin{cases} \tau_1 - TOA_1 = f_d/K, \\ \tau_2 - TOA_2 = -f_d/K, \\ TOA_2 - TOA_1 = \Delta T. \end{cases} \tag{5}$$

Considering the influence of factors such as baseband sampling rate and carrier frequency offset, there is an error between the actual time $\widetilde{\tau}_i$ at which the output of the matched filter reaches the MAP and the theoretical time τ_i. We call this error the peak error and represent it as $e_i = \widetilde{\tau}_i - \tau_i$. By substituting it into Equation (5), we can obtain the measurement formula for TOA1 as follows:

$$TOA_1 = -\frac{e_1 + e_2}{2} + \frac{\widetilde{\tau}_1 + \widetilde{\tau}_2 - \Delta T}{2}. \tag{6}$$

The measurement formula of TOA_1 contains an error term e_i. If e_i is not considered, the maximum measurement error of TOA_1 can reach half of the baseband sampling interval. To achieve high-precision timing, the correction method for e_i is provided in Section 3.2.4. Additionally, based on Equation (5), the measurement formula for carrier frequency offset can also be derived as follows:

$$f_d = \left(\frac{e_2 - e_1}{2} + \frac{\widetilde{\tau}_1 - \widetilde{\tau}_2 + \Delta T}{2} \right) K \tag{7}$$

3.2.4. Peak Error Correction

In this section, we derive a theoretical correction equation for e_i. Using this equation to correct the peak error can improve the timing accuracy of the receiver and the measurement accuracy of the carrier frequency offset.

Let $P_{i,j} (i = 1, 2, j = -1, 0, 1)$ represent the three peaks near the MAP of the ith matched filter, as shown in Figure 9: $P_{i,0}$ represents the MAP, and its output time is $\widetilde{\tau}_i$; $P_{i,-1}$ represents the output peak that is one sampling interval ahead of $P_{i,0}$, and its output time is $\widetilde{\tau}_i - 1/f_s$, where f_s is the baseband sampling rate; and $P_{i,1}$ represents the output peak that is one sampling interval behind $P_{i,0}$, and its output time is $\widetilde{\tau}_i + 1/f_s$.

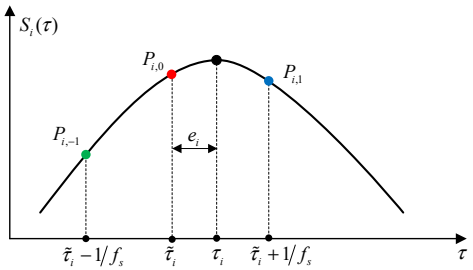

Figure 9. Schematic of the peak value distribution of the matched filtering.

According to the FD-TS characteristic of the Chirp signal, we can obtain $\tau_i = (-1)^{i-1} f_d/K$. Because $\widetilde{\tau}_i = \tau_i + e_i$, by referring to Equation (2), $P_{i,j}$ can be expressed as follows:

$$\begin{aligned} P_{i,j} &= A \left\| \int_0^T \exp\left[j2\pi \left(-f_d t + (-1)^{i-1} K \left((-1)^{i-1} f_d/K + e_i + j/f_s \right) t \right) \right] \mathrm{d}t \right\| \\ &= A \left\| \int_0^T \exp\left[j2\pi \left((-1)^{i-1} K (e_i + j/f_s) \right) t \right] \mathrm{d}t \right\|. \end{aligned} \tag{8}$$

Since the Chirp signal is a pulse signal with a duration of T. When the carrier frequency offset is not zero, according to the FD-TS characteristic, at the time when the MAP is output by the matched filter, only part of the Chirp signal enters the matched filter. Therefore, there must be a deviation between the integral value of Equation (8) and the actual value of $P_{i,j}$. We call this deviation the truncation deviation. To eliminate this deviation, the integral interval can be truncated before and after by T_{cut}. At this time, the integral interval changes from $[0, T]$ to $[T_{cut}, T - T_{cut}]$. Then, Equation (8) can be rewritten as follows:

$$P_{i,j} = A\left\| \int_{T_{cut}}^{T-T_{cut}} \exp\left[\mathrm{j}2\pi\left((-1)^{i-1}K(e_i + j/f_s)\right)t\right]\mathrm{d}t \right\| = A\frac{\sin\left(m_i + k_{i,j}\right)}{\sin\left[\left(m_i + k_{i,j}\right)/\left((T - 2T_{cut})f_s\right)\right]}, \tag{9}$$

where

$$k_{i,j} = (-1)^{i-1}\pi K(T - 2T_{cut})j/f_s, m_i = (-1)^{i-1}\pi K(T - 2T_{cut})e_i. \tag{10}$$

As long as it is ensured that $T_{cut} \geq f_d/K$, the truncation deviation can be eliminated. Since $j = -1, 0, 1$ and $e_i \leq 1/(2f_s)$, it is easy to obtain $\left|\left(m_i + k_{i,j}\right)/\left((T - 2T_{cut})f_s\right)\right| \leq 1.5\pi K/f_s^2$. Therefore, when $f_s \gg \sqrt{1.5\pi K}$, $P_{i,j}$ can be further expressed as follows:

$$P_{i,j} = a\frac{\sin\left(m_i + k_{i,j}\right)}{m_i + k_{i,j}}, \tag{11}$$

where $a = A(T - 2T_{cut})f_s$. According to Equation (11), we can obtain the following:

$$a^{-1}P_{i,0} = \frac{\sin(m_i)}{m_i}, \tag{12}$$

$$a^{-1}P_{i,1} = \frac{\sin(m_i + k_{i,1})}{m_i + k_{i,1}}, \tag{13}$$

$$a^{-1}P_{-1}^{l} = \frac{\sin(m_i - k_{i,1})}{m_i - k_{i,1}}. \tag{14}$$

According to Equations (13) and (12), it is easy to obtain the following:

$$a^{-1}P_{i,1}(m_i + k_{i,1}) = a^{-1}P_{i,0}m_i\cos(k_{i,1}) + \cos(m_i)\sin(k_{i,1}). \tag{15}$$

Similarly, according to Equations (14) and (12), we can obtain the following:

$$a^{-1}P_{-1}^{l}(m_i - k_{i,1}) = a^{-1}P_{i,0}m_i\cos(k_{i,1}) - \cos(m_i)\sin(k_{i,1}). \tag{16}$$

According to Equations (15) and (16), m_i can be further expressed as follows:

$$m_i = \frac{k_{i,1}(P_{i,1} - P_{i,-1})}{2P_{i,0}\cos(k_{i,1}) - P_{i,1} - P_{i,-1}}. \tag{17}$$

Then, substituting Equation (10) into Equation (17), the theoretical correction formula for e_i can be obtained, which is expressed as follows:

$$e_i = \frac{(P_{i,1} - P_{i,-1})/f_s}{2P_{i,0}\cos[\pi K(T - 2T_{cut})/f_s] - P_{i,1} - P_{i,-1}}. \tag{18}$$

Before correcting the peak error, we can first assume that it is zero and calculate the coarse value of the carrier frequency offset according to Equation (7). Then, we adjust the local clock to make $f_d \leq T_{cut}K$, thereby eliminating the truncation deviation. Finally, we calculate the peak error according to Equation (18). Of course, it is also possible to evaluate the maximum carrier frequency offset that may exist in the receiver in advance and then design a sufficiently large T_{cut} to ensure $T_{cut} \geq f_d/K$.

3.3. Parameter Design and Performance Anslysis

At the transmitting end, we know that the time interval between the transmission start time of the $C_1(t)$ signal and the transmission start time of the $C_2(t)$ signal is ΔT. Under ideal conditions, the maximum peak relative time interval $\Delta\widetilde{\tau}$ at the receiving end is equal to ΔT. Considering that several multipath signals exist in the shortwave channel, these signals are likely to cause changes in $\Delta\widetilde{\tau}$. Additionally, considering the time shift of the correlation peak caused by the carrier frequency offset, the value interval of $\Delta\widetilde{\tau}$ at this time can be expressed as $\mathbf{R} = [\Delta T - \tau_{\max} - f_d/K, \Delta T + \tau_{\max} + f_d/K]$, where $\tau_{\max}$ is the maximum multipath delay.

According to Section 3.1.4, if the time signal being broadcast is the UTC signal, then $\Delta T = T_S - T$; if the time signal being broadcast is the UT1 time signal, then $\Delta T = T$. By substituting the two cases of ΔT into $\mathbf{R}$, respectively, the decision domain of the UTC signal and the decision domain of the UT1 time signal can be obtained as follows:

$$\begin{aligned} \mathbf{R}_{\mathrm{UTC}} &= [T_S - T - \tau_{\max} - f_d/K, T_S - T + \tau_{\max} + f_d/K], \\ \mathbf{R}_{\mathrm{UT1}} &= [T - \tau_{\max} - f_d/K, T + \tau_{\max} + f_d/K]. \end{aligned} \tag{19}$$

Evidently, to be able to correctly capture and identify the two time signals of $\mathbf{R}_{\mathrm{UTC}}$ and $\mathbf{R}_{\mathrm{UT1}}$, a basic requirement is that $\mathbf{R}_{\mathrm{UTC}}$ and $\mathbf{R}_{\mathrm{UT1}}$ must not have an intersection, i.e., it is required that $T_S - T - \tau_{\max} - f_d/K > T + \tau_{\max} + f_d/K$. Then, we can obtain the following equation:

$$T < \frac{T_S}{2} - \tau_{\max} - f_d/K = \frac{T_S/2 - \tau_{\max}}{1 + f_d/B}. \tag{20}$$

Generally speaking, to control the manufacturing cost, shortwave timing receivers usually use normal temperature crystal oscillators with poor performance. The output frequency stability is generally 1–20 ppm. Taking the nominal frequency of 10 MHz as an example, f_d can reach up to 200 Hz at most. In addition, this paper assumes that $\tau_{\max}$ is 6 ms. According to Equation (20), it is easy to obtain $T < 33.2$ ms. To obtain a certain margin, we finally design T as 32 ms. Based on this, we can perform the following calculation: $\mathbf{R}_{\mathrm{UTC}} = [25.2\ \mathrm{ms}, 38.8\ \mathrm{ms}]$, $\mathbf{R}_{\mathrm{UT1}} = [41.2\ \mathrm{ms}, 54.8\ \mathrm{ms}]$, and $K = 250\ \mathrm{kHz/s}$. Furthermore, we determine the spread spectrum gain $G = 10\log_{10}(BT) = 24$ dB of $C_1(t)$ and $C_2(t)$, and the minimum multipath resolution $\tau_{\min} = 1/B = 125$ μs.

According to the above parameter design, a single Chirp signal in DCTDCM can have a spread spectrum gain of 24 dB, which greatly improves the anti-interference reception performance of shortwave time signals. At the same time, it also has a multipath resolution capability of at least 125 μs, which improves the anti-multipath fading performance of shortwave time signals.

Next, the performance of DCTCDM is further explained through simple examples.

In the absence of multiple interferences, Figure 10 shows the autocorrelation functions of AM and DCTCDM. The autocorrelation peak of the AM baseband signal fluctuates significantly and is easily affected by noise, leading to the receiver locking on the wrong peak. In contrast, the autocorrelation peak of the DCTCDM baseband signal is sharper, less affected by noise interference, and has high signal synchronization accuracy, which is crucial for precise timing.

When there are two-path signals (power-related with a relative time delay difference of 500 μs), Figure 11 presents the autocorrelation functions of AM and DCTCDM. The AM baseband signal is easily affected by multipath interference and causes severe fading. The DCTCDM baseband signal has multipath resolution capability and can effectively resist multipath fading. It is more suitable for shortwave channels with severe multipath interference, thereby improving the reliability of shortwave timing services.

Figure 12 briefly describes the process by which a spread spectrum receiver realizes the reception of anti-Narrowband Interference Signals (NIS). When the spread spectrum signal (target signal) enters the radio frequency end of the receiver, its spectrum is suppressed by the NIS signal. After correlation despreading, the spectrum of the target signal is

concentrated, while the spectrum of the NIS is broadened and the in-band energy is reduced. If the spread spectrum gain of the target signal is large enough, after narrowband filtering, the energy of the target signal is much greater than that of the NIS signal. Therefore, when the receiver receives the DCTCDM signal, it can effectively suppress the in-band NIS caused by the spectrum leakage of radio signals at nearby frequencies. This is also of crucial importance for maintaining the reliability of the shortwave timing system.

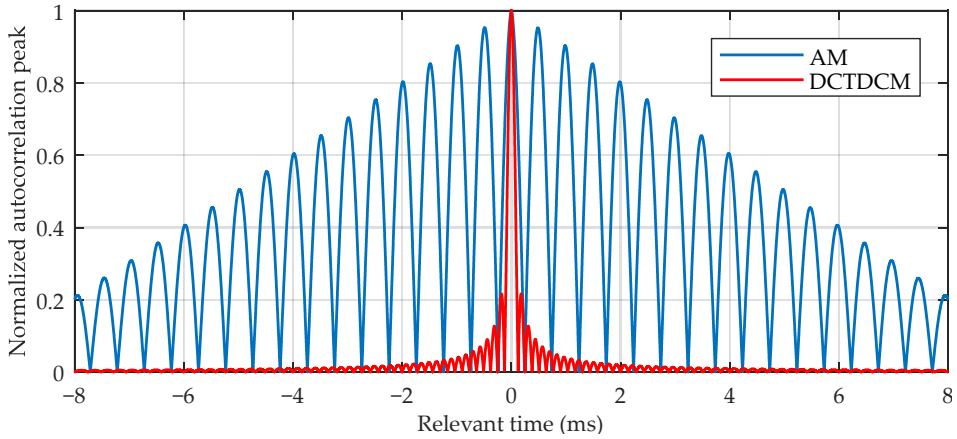

Figure 10. Autocorrelation functions of AM and DCTDCM without multipath interference.

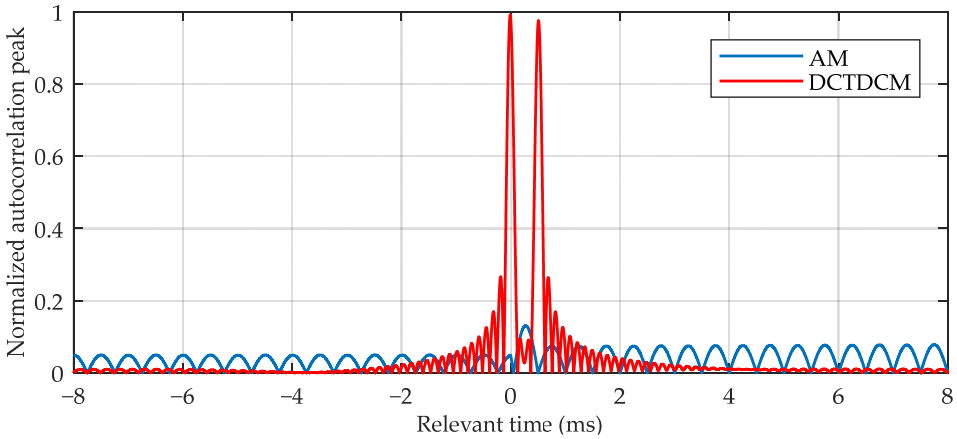

Figure 11. Autocorrelation functions of AM and DCTDCM with multipath interference.

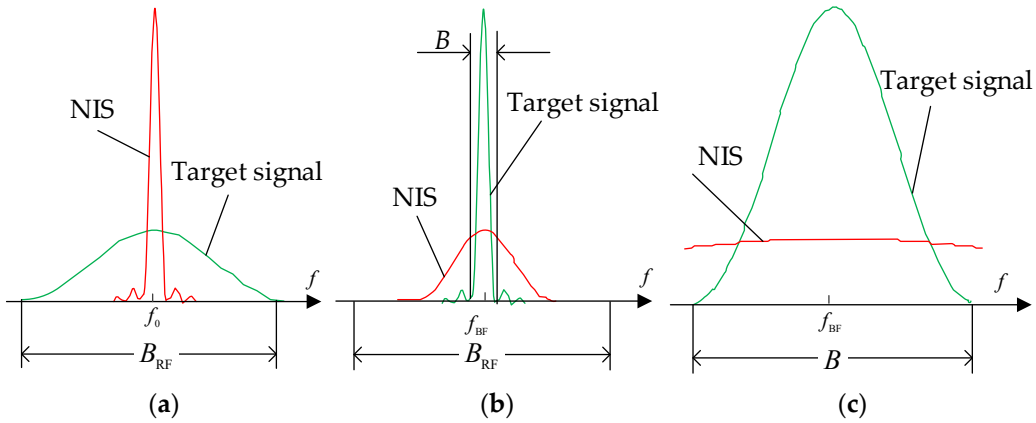

Figure 12. Schematic spectra in key parts of a spread spectrum receiver: (**a**) is the spectrum at the RF input terminal; (**b**) is the spectrum after correlation dispreading; (**c**) is the spectrum after narrowband filtering.

4. Results

4.1. Experimental Method

The geographic diversity of the test locations plays a crucial role in understanding the performance of the modulation schemes under different environmental and propagation conditions, such as those encountered in rural, urban, and coastal areas, which are essential for shortwave time systems. To verify the effectiveness of our work, from 16 September 2022 to 30 October 2022, we conducted a field test comparing the receiving performance of the DCTDCM and the AM schemes in Pucheng County, Luonan County, Xi'an City, Xuyi County, Changchun City, Sanya City, and Kashgar City within China. The detailed information for the test locations is shown in Table 1.

Table 1. Detailed information of test location.

Test Location	Mark of Test Location	Distance from the Broadcasting Station (km)
Luyang Lake in Pucheng County, Weinan City, Shaanxi Province.	TL1	13.9
Bao'an Town, Luonan County, Luonan City, Shaanxi Province.	TL2	94.8
Xi'an Science Park, Xi'an City, Shaanxi Province.	TL3	119.1
Xuyi Observation Station of Purple Mountain Observatory	TL4	859.3
Changchun Satellite Observing Station, National Astronomical Observatories, Chinese Academy of Sciences.	TL5	1678.2
Sanya Branch of the 725th Institute of China Shipbuilding Industry Corporation.	TL6	1852.8
Kashgar Observation Station of Xinjiang Astronomical Observatory.	TL7	2994.8

The test data for this actual measurement experiment primarily consist of UTC difference measurement data. These data involve the receiver capturing and recognizing the UTC signal, then performing timing and outputting the local 1 Pulse Per Second (1 PPS), and subsequently measuring the time difference between the local 1 PPS and the reference 1 PPS. By counting the number of valid values and the standard deviation in the UTC difference measurement data, two performance indicators—time signal availability rate and timing accuracy—are obtained. These indicators are used to evaluate and compare the receiving performance of the two modulated time signals. In this study, the valid value for the UTC difference measurement refers to those with an absolute value less than 10 ms.

The time signal availability rate reflects the anti-interference performance of the time signals, while timing accuracy reflects the peak detection accuracy (or the measurement accuracy of signal arrival time). The time signal availability rate is denoted as λ_{tc}, and its statistical formula is as follows:

$$\lambda_{tc} = \frac{N_{tc\_valid}}{T_{static} \times 2/3} \times 100 = \frac{N_{tc\_valid}}{T_{static}} \times 1.5 \times 100, \quad (21)$$

where T_{static} (in seconds) is the statistical time, N_{tc_valid} is the number of valid values of UTC difference measurements within T_{static}, and the coefficient 3/2 is the broadcast frequency of UTC signals (within 30 min, UTC signals are broadcast for 20 min).

In Section 4.2, our test platform is introduced in detail. In Section 4.3, the test data obtained over a short period of time are analyzed. In Section 4.4, the test data for a long period of time are analyzed.

4.2. Test Platform

To support the implementation of actual measurement experiments, we have developed four new shortwave timing exciters and six test receivers to build the test platform for the actual measurement experiment. As shown in Figure 13, the new shortwave timing

exciter generates the BPM shortwave timing signal containing DCTDCM and AM signals according to the overall scheme given in Section 3.1.1. The test receivers can simultaneously receive the two modulated time signals described above.

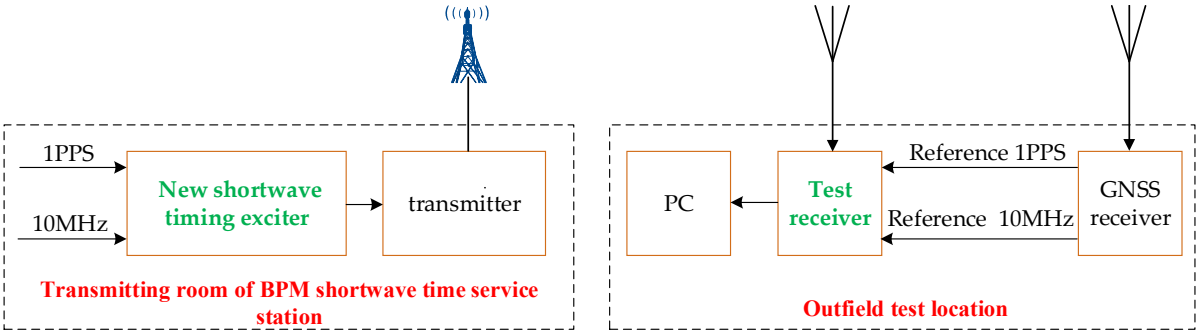

Figure 13. Schematic of the test platform.

The four exciters developed are all deployed in the BPM shortwave timing broadcast room to replace the original exciters. Among the six test receivers developed, one is used for short-term testing, while the other five are set up at fixed locations for long-term testing. The time reference used by the test receiver is provided by the GNSS receiver. Figure 14 shows some of our test platforms and test personnel. In particular, Figure 14a shows the deployment of the new shortwave timing exciter. Figure 14b is a group photo of some test personnel in front of the BPM shortwave timing broadcast console. Figure 14c shows the test receiver and receiving antenna at test location TL1. Figure 14d shows the test personnel observing and analyzing the test results at test location TL2.

(**a**) (**b**)

(**c**) (**d**)

Figure 14. Test platform and test personnel: (**a**) Photograph of the new exciter deployed in the BPM shortwave timing broadcast room. (**b**) Group photo of some test personnel. (**c**) Photograph of the test receiver at LT1. (**d**) Test personnel observing the test data at TL2.

4.3. Short-Term Tests

We conducted the short-term tests at test locations TL1, TL2, TL3, and TL6. The test data are shown in Figures 15–18, respectively. These test data are summarized in Table 2.

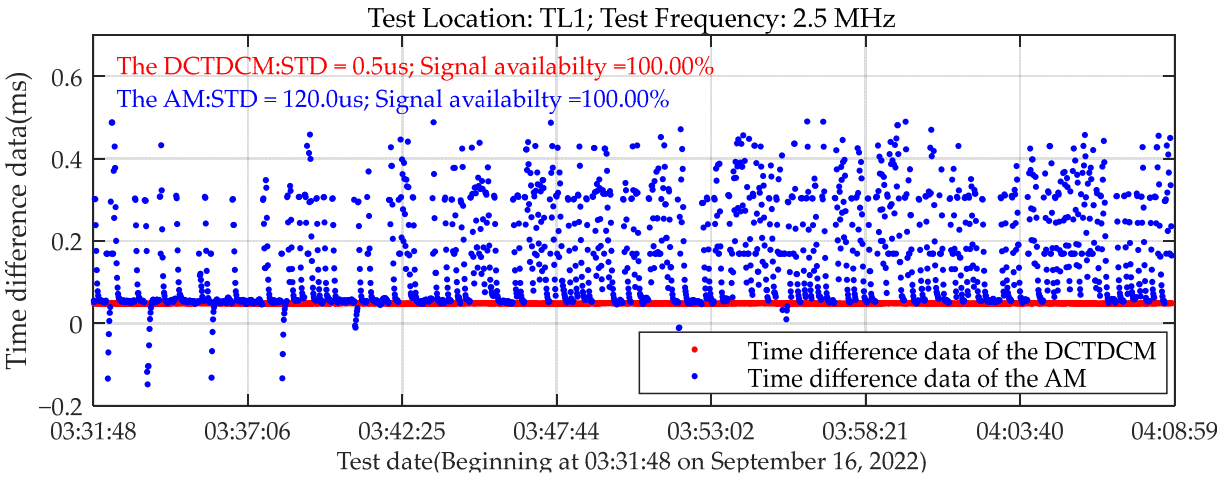

Figure 15. Short-term test data of test location LT1.

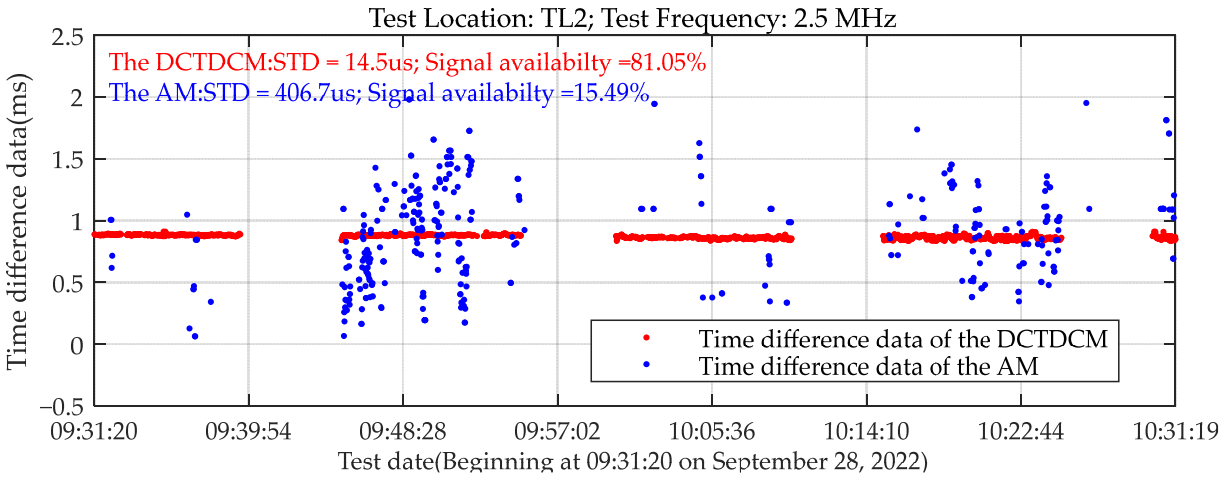

Figure 16. Short-term test data of test location LT2.

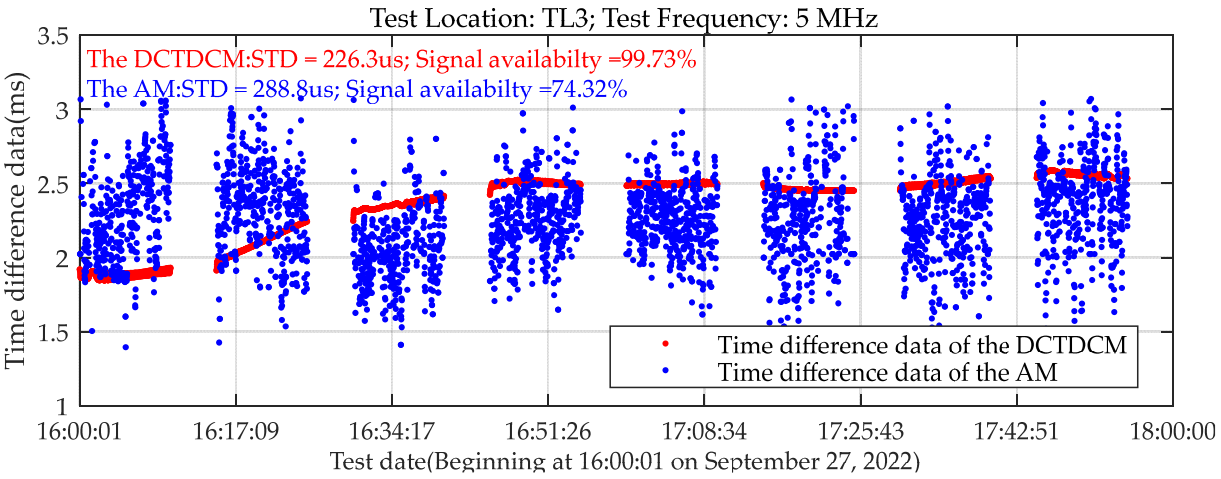

Figure 17. Short-term test data of test location LT3.

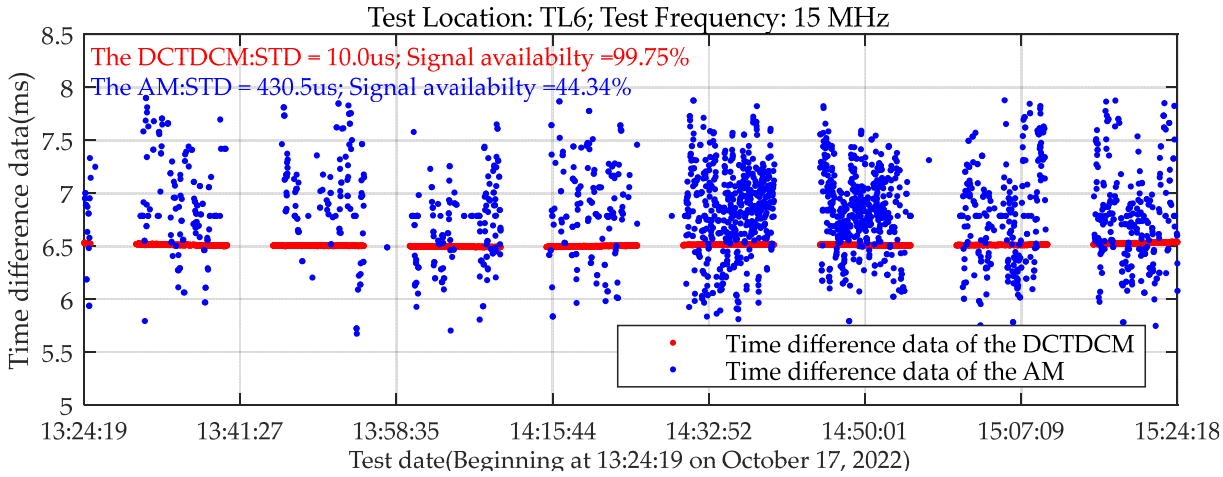

Figure 18. Short-term test data of test location LT6.

Table 2. Test results for short periods.

Test Location	Test Frequency	Test Duration	Time Signal Availability Rate		Timing Accuracy	
			DCTDCM	AM	DCTDCM	AM
TL1	2.5 MHz	Twenty-three minutes.	100%	100%	0.5 μs	120 μs
TL2	2.5 MHz	One hour.	81.05%	15.49%	14.5 μs	406.7 μs
TL3	5 MHz	Two hours.	99.73%	74.32%	226.3 μs	288.8 μs
TL6	15 MHz	Two hours.	99.75%	44.34%	10.0 μs	430.5 μs

The test conducted at test location TL1 is a short-distance test, which is mainly used to verify whether our test platform functions properly. As shown in the test results in Table 2, the availability rates of both time signal modulation methods are 100%, indicating that the exciters and test receivers we developed operate correctly.

The test results demonstrate that, except for test location TL1, at the other three test locations, the time signal availability rate of the DCTDCM is significantly better than that of AM. Moreover, except for test location TL3, the timing accuracy of DCTDCM is significantly better than that of the existing AM at the other three test locations. This demonstrates that, compared to the existing AM signal, the anti-interference receiving performance and peak detection accuracy of the DCTDCM signal are significantly improved, verifying the effectiveness of the work presented in this paper.

At test location TL3, although the timing accuracy of the two modulation methods is comparable, as seen in Figure 17, the test data for DCTDCM more clearly reflect changes in signal propagation delay due to ionospheric variations. This will aid in the subsequent in-depth study of the refined characteristics of the shortwave ionosphere. This advantage also highlights the higher peak detection accuracy of the DCTDCM signal.

4.4. Long-Term Tests

We conducted long-term tests at six test locations: TL3, TL4, TL5, TL6, and TL7. The test period was from 1 October 2022 to 30 October 2022. The test frequencies were 5 MHz and 15 MHz. The 5 MHz frequency was tested throughout the day for a total of 30 days. To minimize the impact on existing shortwave users, no tests were conducted during the day for the 15 MHz signal, which is normally broadcast. The evening (09:30–01:30) was selected for testing the 15 MHz signal, with a total of 29 d of testing (the 15 MHz signal was not tested on the evening of 6 October 2022).

The long-term test data for test locations TL3, TL4, TL5, TL6, and TL7 are shown in Figures 19–23, respectively. From these figures, it is evident that regardless of the test

location and test frequency, the time signal availability rate of the DCTDCM is significantly better than that of AM.

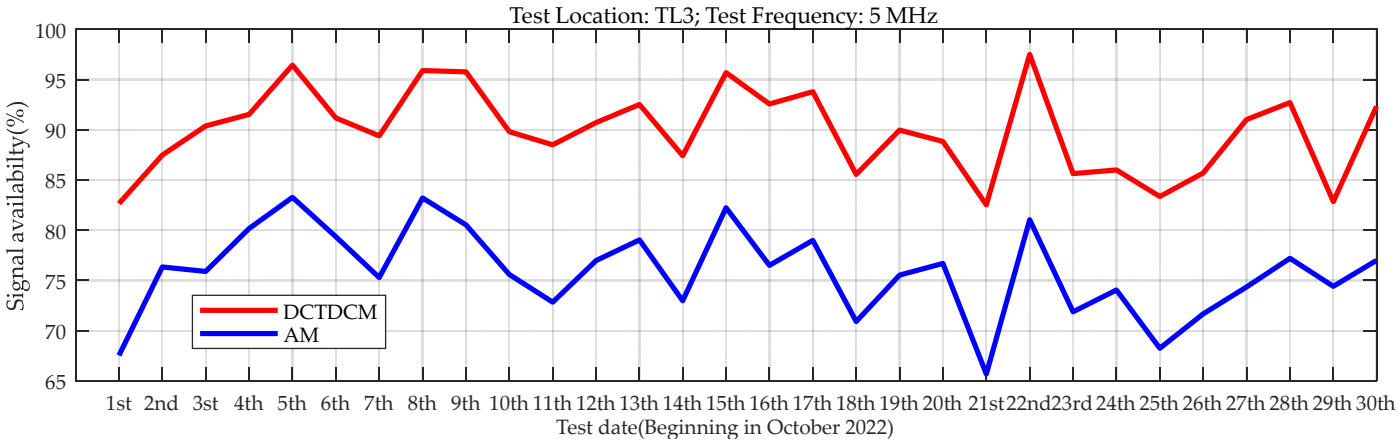

Figure 19. Long-term and short-term test data of test location LT3.

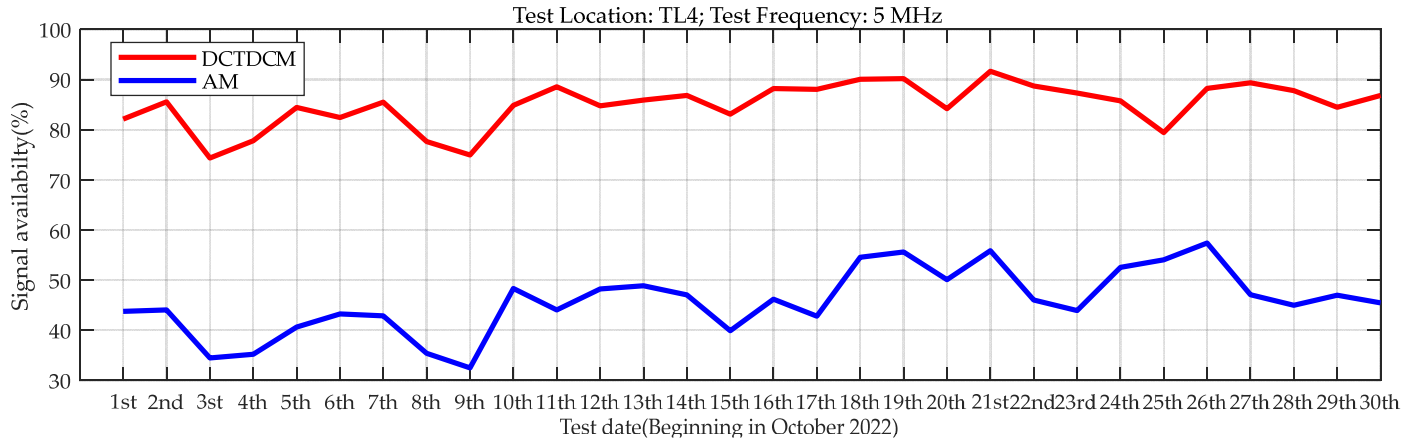

Figure 20. Long-term and short-term test data of test location LT4.

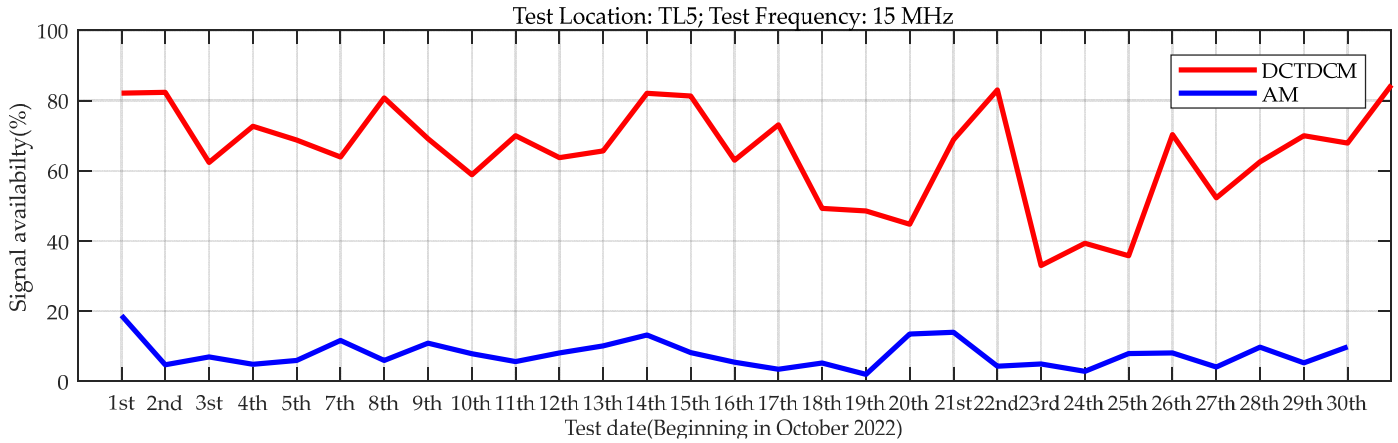

Figure 21. Long-term and short-term test data of test location LT5.

For the test data from TL3, the time signal availability rate of AM ranges from 66% to 83%, with 21 d below 77%. The availability rate for DCTDCM is between 87% and 98%, with 28 d above 91%.

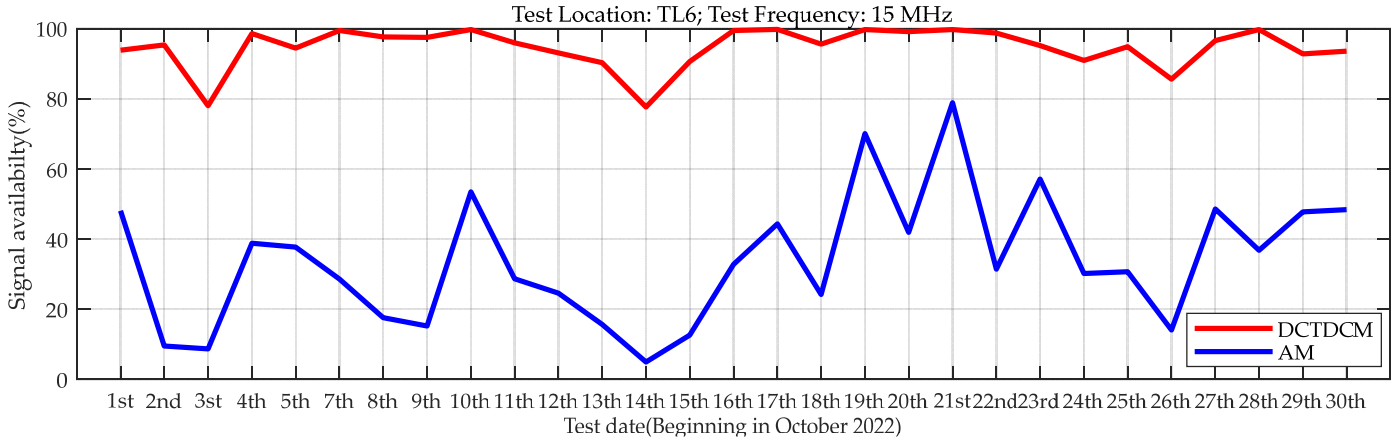

Figure 22. Long-term and short-term test data of test location LT6.

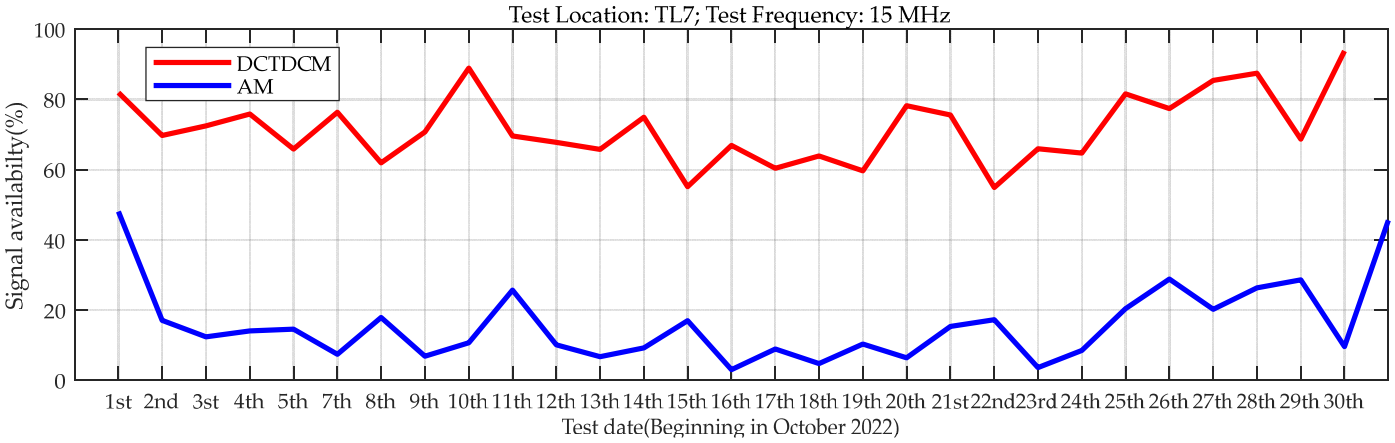

Figure 23. Long-term and short-term test data of test location LT7.

For the test data from TL4, the time signal availability rate of AM ranges from 33% to 57%, with 23 d below 49%. The availability rate for DCTDCM is between 74% and 92%, with 25 d above 80%.

For the test data from TL5, the time signal availability rate of AM ranges from 2% to 19%, with 25 d below 13%. The availability rate for DCTDCM is between 33% and 84%, with 23 d above 50%.

For the test data from TL6, the time signal availability rate of AM ranges from 5% to 79%, with 26 d below 54%. The availability rate for DCTDCM is between 75% and 100%, with 27 d above 85%.

For the test data from TL7, the time signal availability rate of AM ranges from 3% to 46%, with 28 d below 31%. The availability rate for DCTDCM is between 55% and 94%, with 23 d above 65%.

This data comparison clearly demonstrates that the anti-interference receiving performance of the DCTDCM proposed in this paper is significantly better than that of the existing AM time signal. Thus, the effectiveness of our work is once again verified.

5. Discussion

The shortwave channel is a low-quality variable-parameter channel. With the rapid development of the information society, various types of interference in the shortwave channel have become increasingly problematic. The existing AM used in shortwave time services has struggled to maintain the time service performance required by the system. Considering the autonomy and diversity of time–frequency services in China and the

strategic need to build a national resilient time service system, it is essential to promote the advancement of BPM shortwave time service technology.

When developing new shortwave time service technologies, the primary objective should be to enhance the anti-interference capability of shortwave time service signals, thereby improving the reliability and availability of shortwave time service systems. The introduction of spread spectrum technology into shortwave time services, while maintaining compatibility with existing transmission systems and users, is undoubtedly the most effective technical approach to achieving these goals. The main contributions and future work plans of this paper are as follows.

(1) Theoretical Innovation and Contributions

This paper conducts in-depth research on Chirp signals. After comparing them with traditional DSSS signals, it clearly elaborates on their multiple advantages. Through analysis, it is concluded that Chirp signals have a flatter spectrum and more concentrated energy distribution. The sharper main lobe of its autocorrelation peak helps to more accurately identify and extract signals at the receiving end, enhancing the accuracy of signal processing. Stronger multipath resolution and excellent resistance to carrier frequency offset enable signals to transmit more stably in complex shortwave channel environments.

We have studied the FD-TS characteristic of Chirp signals and revealed the relationship between the timing of Chirp's autocorrelation peak and carrier frequency offset and chirp rate, providing a key theoretical basis for the subsequent DCTDCM scheme. This in-depth exploration based on the intrinsic characteristics of signals makes the theory of signal modulation and processing richer and more complete.

The proposal of the DCTDCM scheme is one of the core innovation points of this paper. Using two Chirp signals with opposite chirp rates to achieve the broadcasting of UTC and UT1 realizes an innovative breakthrough in the time signal transmission mechanism. This scheme not only innovates the coding and transmission method of time signals but also enables the joint measurement of signal arrival time and carrier frequency offset at the receiving end through ingenious design. This innovative measure partly solves the problems of signal synchronization and frequency compensation in shortwave communication and provides a brand new solution for improving the accuracy and reliability of shortwave time services.

The proposal of the time signal capture and identification method based on MPRTID solves a major problem associated with signal reception in complex shortwave channels. The characteristic of not requiring the setting of a correlation peak threshold makes the receiving method more flexible and adaptable to the actual channel environment. Capturing signals by comparing the autocorrelation peak of the target signal with the cross-correlation peak of the interference signal and adopting a multi-dwell decision strategy to improve the detection probability and reduce false alarm rate theoretically optimizes the signal reception process and improves reception efficiency and accuracy, adding new content to the theory of shortwave signal reception.

Deriving the theoretical correction formula for peak error in signal arrival time measurement is another important contribution of this paper in theoretical research. This formula provides a theoretical basis for further improving the timing accuracy of the receiver in the future, making it possible to accurately measure and process signals in shortwave time services and helping to build a more accurate shortwave communication time service model.

In the parameter design process of DCTDCM, fully considering the characteristics of shortwave channels and carrier frequency offsets and adopting a redundant design concept is an innovative and scientific design method. The achieved spread spectrum gain of 24 dB and multipath resolution capability of at least 125 μs provide quantitative guarantees in theory for improving the anti-interference and anti-multipath fading performance of shortwave time signals. This parameter design concept provides new theoretical guidance for the optimization design of shortwave communication systems and helps to build a more stable and efficient shortwave time service system.

(2) Contributions in Experimental Verification

We independently develop a new shortwave time service exciter and test receiver and build a test platform, which is a work of great practical significance. The development of testing equipment provides a hardware basis for accurately obtaining and analyzing experimental data, enabling research results to be verified in actual environments. At the same time, the construction of the test platform provides a reference example for the construction of experimental environments for subsequent related research and promotes the development of experimental research methods in the field of shortwave time service technology.

We conduct field tests in multiple regions with different geographical environments and climatic conditions in China, including from inland counties to coastal cities, fully considering the diversity of shortwave propagation environments. This wide range of testing makes the research results more universal and persuasive and can fully reflect the performance of DCTDCM in various actual scenarios. It provides rich data references for the application of shortwave time service technology in different regions and environments.

Through detailed comparison of test data, the advantages of DCTDCM over traditional AM are clearly demonstrated. The significant improvement in peak detection accuracy in short-term tests and the continuous superiority of the time signal availability rate in long-term tests provide reliable data support for the improvement of shortwave time service technology. In particular, the clearer reflection of DCTDCM signal data on the propagation delay changes in the shortwave ionosphere not only verifies the correctness of theoretical research results but also provides an effective way to further study shortwave propagation characteristics.

(3) Future Work Plans

As part of the high-precision ground-based time service system project created by the NTSC, more than 100 long-wave time service differential stations will be built in the future, and most of the stations will be co-located with meteorological monitoring stations. Our plans for future work are based on the research results of this paper and use these differential stations to build a relatively complete short-wave time service monitoring system to support research related to space environment and radio wave propagation, especially studying the influence of factors such as ionospheric characteristics, atmospheric noise, and meteorological conditions on the propagation of short-wave signals. This will further promote interdisciplinary innovation in the short-wave field and prompt the rapid development of short-wave communication, time service, and positioning technologies.

6. Conclusions

Currently, as satellite-based timing technologies such as GPS and BDS become increasingly popular research topics, shortwave timing technology has received less attention. However, owing to its irreplaceable advantages—such as long operating distances and survivability in wartime—shortwave timing remains an indispensable method. Although the timing accuracy of the shortwave timing system is not as high as that of GNSS, it serves as a crucial backup for time users, ensuring that "time" is available under extreme conditions. The research presented in this paper has improved both the availability rate of shortwave time signals and the timing accuracy for users, which is of great significance in advancing shortwave timing technology and in supporting the development of the next-generation BPM shortwave timing system.

Author Contributions: Conceptualization, J.Y. and S.L.; methodology, J.Y. and Y.H.; software, J.Y., W.Y. and D.Y.; validation, J.Y., W.Y., D.Y., Y.S., C.Y. and Z.H.; formal analysis, Y.S.; investigation, J.Y. and W.Y.; resources, S.L.; data curation, J.Y. and D.Y.; writing—original draft preparation, J.Y.; writing—review and editing, J.Y. and S.L.; visualization, Z.H. and C.Y.; supervision, S.L. and Y.H.; project administration, S.L.; funding acquisition, J.Y., C.Y. and Y.S. All authors have read and agreed to the published version of the manuscript.

Funding: This research was funded by the Innovation Capability Support Program of Shaanxi (Program No. 2024ZC-KJXX-104) and the open Fund Program of the Laboratory of Science and Technology the Open Fund Program of the Laboratory of Science and Technology on Marine Navigation and Control, China State Shipbuilding Corporation (Grant No. 2023010106) and the Youth Innovation Promotion Association CAS (Grant No. 2021409).

Institutional Review Board Statement: Not applicable.

Informed Consent Statement: Not applicable.

Data Availability Statement: Restrictions apply to the availability of these data. The ownership of data belongs to the National Time Service Center (NTSC). These data can be made available by the corresponding author with the permission of NTSC.

Acknowledgments: The authors would like to thank their colleagues for testing the data provided in this manuscript. We are also very grateful to our reviewers, who provided insight and expertise that greatly assisted the research.

Conflicts of Interest: Author Jiangbin Yuan was employed by the company China State Shipbuilding Corporation. And Author Dafeng Yang was employed by Xi'an Air-Space Electronic Technology Co., Ltd. The remaining authors declare that the re-search was conducted in the absence of any commercial or financial relationships that could be construed as a potential conflict of interest.

References

1. Hua, Y.; Guo, W.; Yan, B.; Xu, Y. Developing status of national time service architecture. *J. Time Freq.* **2016**, *39*, 193–201. [CrossRef]
2. Yuan, J.; Hua, Y.; Li, S.; Yan, W.; Hu, Z. Discussion on the application of OFDM in BPM HF data modulation. *J. Time Freq.* **2019**, *42*, 169–175. [CrossRef]
3. Yuan, J.; Yan, W.; Li, S.; Hua, Y. Demodulation Method for Loran-C at Low SNR Based on Envelope Correlation–Phase Detection. *Sensors* **2020**, *20*, 4535. [CrossRef] [PubMed]
4. Liu, K.; Yuan, J.; Yan, W.; Yang, C.; Guo, W. A Shrink-Branch-Bound Algorithm for eLoran Pseudorange Positioning Initialization. *Remote Sens.* **2022**, *14*, 1781. [CrossRef]
5. Specht, M. Determination of navigation system positioning accuracy using the reliability method based on real measurements. *Remote Sens.* **2021**, *13*, 4424. [CrossRef]
6. Yan, W.; Dong, M.; Li, S.; Yang, C.; Yuan, J.; Hu, Z. An eLoran Signal Cycle Identification Method Based on Joint Time–Frequency Domain. *Remote Sens.* **2022**, *14*, 250. [CrossRef]
7. Zou, Z.; Wang, G.; Li, Z.; Zhai, R.; Li, Y. MFO-Fusion: A Multi-Frame Residual-Based Factor Graph Optimization for GNSS/INS/LiDAR Fusion in Challenging GNSS Environments. *Remote Sens.* **2024**, *16*, 3114. [CrossRef]
8. Cheng, L.; Zhang, S.; Qi, Z.; Wang, X. Research on eLoran Weak Signal Extraction Based on Wavelet Hard Thresholding Processing. *Remote Sens.* **2024**, *16*, 3012. [CrossRef]
9. Yuan, J.; Hua, Y.; Li, S.; Yan, W.; Gao, Y. Study on data modulation for BPM HF based on Chirp signal. *J. Time Freq.* **2019**, *42*, 327–335. [CrossRef]
10. Yuan, J.; Li, S.; Yan, W.; Yang, C.; Hu, Z. A Novel Transmission Scheme of HF Time Signals based on Spread Spectrum System and its Feasibility Analysis. *J. Astronaut. Metrol. Meas.* **2019**, *39*, 38–43.
11. Lai, F.; Wang, C.; Huang, J.; Feng, R.; Gao, X.; Zheng, F. A Novel 3D Non-Stationary Massive MIMO Channel Model for Shortwave Communication Systems. *IEEE Trans. Commun.* **2023**, *71*, 5473–5486. [CrossRef]
12. Wang, Y.; Zhang, Y.; Xie, M. Modeling and simulation of short-wave ionospheric radio channel. *Chin. J. Radio Sci.* **2004**, *19*, 357–361. [CrossRef]
13. Hu, Y.; Wang, C.; Ren, Y.; Zhou, F. High Frequency Channel Multipath Analysis Based on Ionosphere Dispersion. *J. Electron. Inf. Technol.* **2020**, *42*, 2006–2012. [CrossRef]
14. LI, J.; Zeng, X.; Li, G.; Ye, C. Shortwave multichannel information fusion method based on DSmT evidence discount theory. *J. Commun.* **2024**, *45*, 29–40. [CrossRef]
15. Springer, A.; Gugler, W.; Huemer, M.; Koller, R.; Weigel, R. A wireless spread-spectrum communication system using SAW chirped delay lines. *IEEE Trans. Microw. Theory Techn.* **2001**, *49*, 754–760. [CrossRef]
16. Wen, R.; Sha, X.; Zhang, X. An Accurately Synchronous Method Using Chirp Signal in Fractional Fourier Domain. *J. Xi'An JiaoTong Univ.* **2009**, *43*, 80–84. Available online: https://zkxb.xjtu.edu.cn/#/digest?ArticleID=1258 (accessed on 7 June 2016).
17. Liu, H. Novel Synchronization Method for Chirp Communication System. *J. Univ. Electron. Sci. Technol. China* **2009**, *38*, 913–926. [CrossRef]
18. Wang, Y.; Cheng, Y.; Yin, j.; Cai, P.; Zhang, Y. Research on orthogonal multi-carrier underwater acoustic communication system based on fractional Fourier transform. *J. Commun.* **2012**, *33*, 162–170.
19. Oh, D.; Kwak, M.; Chong, J. A Subspace-Based Two-Way Ranging System Using a Chirp Spread Spectrum Modem, Robust to Frequency Offset. *IEEE Trans. Wirel. Commun.* **2012**, *11*, 1478–1487. [CrossRef]

20. Pei, H.; Thushara, D.; Tharaka, A. Multiple Target Localization Using Wideband Echo Chirp Signals. *IEEE Trans. Signal Process.* **2013**, *61*, 4077–4089. [CrossRef]
21. Azim, A.W.; Bazzi, A.; Shubair, R.; Chafii, M. Dual-mode chirp spread spectrum modulation. *IEEE Wirel. Commun. Lett.* **2022**, *11*, 1995–1999. [CrossRef]
22. Qian, Y.; Ma, L.; Liang, X. Symmetry Chirp Spread Spectrum Modulation Used in LEO Satellite Internet of Things. *IEEE Commun. Lett.* **2018**, *22*, 2230–2233. [CrossRef]
23. Sedighe, S.; Mahmoud, F. Detectability of Chaotic Direct-Sequence Spread-Spectrum Signals. *IEEE Wirel. Commun.Lett.* **2015**, *4*, 589–592. [CrossRef]
24. Masmoudi, A.; Bellili, F.; Affes, S.; Ghrayeb, A. Maximum Likelihood Time Delay Estimation From Single-and Multi-Carrier DSSS Multipath MIMO Transmissions for Future 5G Networks. *IEEE Trans.Wireless Commun.* **2017**, *16*, 4851–4865. [CrossRef]
25. Xing, Y.; Hu, A.; Zhang, J.; Peng, L.; Li, G. On Radio Frequency Fingerprint Identification for DSSS Systems in Low SNR Scenarios. *IEEE Commun. Lett.* **2018**, *22*, 2326–2329. [CrossRef]
26. Tayebi, A.; Berber, S.; Swain, A. Security Enhancement of Fix Chaotic-DSSS in WSNs. *IEEE Commun. Lett.* **2018**, *22*, 816–819. [CrossRef]
27. Choi, H.; Moon, H. Blind Estimation of Spreading Sequence and Data Bits in Direct-Sequence Spread Spectrum Communication Systems. *IEEE Access* **2020**, *8*, 148066–148074. [CrossRef]
28. Haab, D.B.; Sego, T.C.; Holschuh, T.V.; Moradi, H.; Farhang-Boroujeny, B. Multicode Signaling in a Filter Bank Multicarrier Spread Spectrum System and Its Application to HF Communications. *IEEE Open J. Commun. Soc.* **2023**, *4*, 442–455. [CrossRef]
29. Yu, X.; Cai, X.; Xu, W.; Sun, H.; Wang, L. Differential Phase Shift Keying-Aided Multi-Mode Chirp Spread Spectrum Modulation. *IEEE Wirel. Commun. Lett.* **2023**, *13*, 298–302. [CrossRef]
30. Yu, F.; Chen, G.; Cao, J. Parameter Estimation of LFM Signal Based on the Chirp-Fourier Transform. *J. Electron. Meas. Instrum.* **2003**, *17*, 75–79.
31. Wu, L.; Wei, X.; Yang, D.; Wang, H.; Li, X. ISAR Imaging of Targets With Complex Motion Based on Discrete Chirp Fourier Transform for Cubic Chirps. *IEEE Trans. Geosci. Remote Sens.* **2012**, *50*, 4201–4212. [CrossRef]
32. Zhang, K.; Coutts, F.K.; Thompson, J. Non-Coherent Discrete Chirp Fourier Transform for Modulated LFM Parameter Estimation. In Proceedings of the 2022 Sensor Signal Processing for Defence Conference (SSPD), London, UK, 13–14 September 2022. [CrossRef]
33. Ranjan, R.; Jindal, N.; Singh, A.K. Fractional S-Transform and Its Properties: A Comprehensive Survey. *Wirel. Pers. Commun.* **2020**, *113*, 2519–2541. [CrossRef]
34. Petrov, N.; Yarovoy, A.G. Fractional Fourier Transform Receiver for Modulated Chirp Waveforms. *IEEE Trans. Microw. Theory Techn.* **2023**, *71*, 818–826. [CrossRef]
35. Li, Z.; Gao, Z.; Chen, L.; Gao, J.; Xu, Z. The Synchrosqueezed Method and Its Theory-Analysis-Based Novel Short-Time Fractional Fourier Transform for Chirp Signals. *Remote Sens.* **2024**, *16*, 1173. [CrossRef]
36. Aldimashki, O.; Serbes, A. Performance of Chirp Parameter Estimation in the Fractional Fourier Domains and an Algorithm for Fast Chirp-Rate Estimation. *IEEE Trans. Aerosp. Electron. Syst.* **2020**, *56*, 3685–3700. [CrossRef]
37. Xie, G. *Principles of GPS and Receiver Design*, 1st ed.; Publishing Home of Electronics Industry: Beijing, China, 2011; pp. 358–361.